On limiting for higher order discontinuous Galerkin method for 2D Euler equations

Juan Pablo Gallego-Valencia [*], Christian Klingenberg [†], Praveen Chandrashekar [‡]

October 6, 2015

Abstract

We present an implementation of discontinuous Galerkin method for 2-D Euler equations on Cartesian meshes using tensor product Lagrange polynomials based on Gauss nodes. The scheme is stabilized by a version of the slope limiter which is adapted for tensor product basis functions together with a positivity preserving limiter. We also incorporate and test shock indicators to determine which cells need limiting. Several numerical results are presented to demonstrate that the proposed approach is capable of computing complex discontinuous flows in a stable and accurate fashion.

Keywords: Partial Differential Equations, Conservation Laws, discontinuous Galerkin method, Limiters, compressible Euler equations, shock indicator.

1 Introduction

A high order implementation of the Runge-Kutta discontinuous Galerkin method (RKDG) applied to the compressible hydrodynamical model (Euler equations of gas dynamics) is presented. It is well known that systems of conservation laws admit non-smooth solutions. Therefore high order approximations may generate unphysical oscillations around discontinuities. A way to control these oscillations needs to be devised without affecting the accuracy in smooth regions. A common technique used for this purpose consists in applying a post-processing slope limiter [1]. Another approach is to identify cells in which shocks may be present [2, 3] and to apply the slope limiter only in those cells, thus also improving the efficiency of the scheme. For stability reasons, it is also necessary to ensure the positivity of variables like density and pressure during the simulation. This can be achieved through the implementation of a positivity preserving limiter [4]. In this work we develop a RKDG code using tensor product Lagrange polynomials and modify the usual slope limiter for this case. We also implement and test shock indicators and positivity limiters for tensor product polynomials. Numerical simulations show that the schemes selected have a satisfactory performance when implemented over different two-dimensional test cases, and the shock indicator is able to reliably identify shock regions thus leading to a stable scheme.

[*]speaker, Dept. of Mathematics, Würzburg University, Germany,
[†]Dept. of Mathematics, Würzburg University, Germany,
[‡]TIFR Center for Applicable Mathematics, Bangalore, India

2 Compressible Euler equations

Consider the Euler equations as the two dimensional compressible hydro-dynamical model of conservation laws given by

$$\begin{aligned} (\rho)_t + \nabla_{\mathbf{x}} \cdot (\rho \mathbf{u}) &= 0 \\ (\rho \mathbf{u})_t + \nabla_{\mathbf{x}} \cdot (\rho \mathbf{u} \otimes \mathbf{u} + P) &= 0 \\ (E)_t + \nabla_{\mathbf{x}} \cdot ((E + P)\,\mathbf{u}) &= 0 \end{aligned} \tag{1}$$

where a closure condition between pressure and energy is given by ideal gas model as $E = \frac{P}{\gamma - 1} + \frac{1}{2}\rho|\mathbf{u}|^2$. For the state vector $\boldsymbol{w} = [\rho, \rho u_1, \rho u_2, E]^T$, the admissible set of solutions $\mathcal{U}_{\text{ad}}$ is given by

$$\mathcal{U}_{\text{ad}} = \{\boldsymbol{w} \in \mathbb{R}^4 : \rho(\boldsymbol{w}) > 0, \quad P(\boldsymbol{w}) > 0\} \tag{2}$$

3 Discontinuous Galerkin discretization

For the finite element discretization space $\mathbb{Q}_k$ a tensorial product polynomial basis will be used. In this case the number of terms of the polynomial basis is given by $\dim(\mathbb{Q}_k) = (k+1)^d$, where k is the order of the one dimensional polynomial and d is the dimension of the space domain. Then any two dimensional polynomial $p \in \mathbb{Q}_k$ is of the form

$$p(x, y) = \sum_{0 \leq i,j \leq k} p_{ij} x^i y^j. \tag{3}$$

Calling τ_ℓ as a single cell in the domain, a disjoint domain decomposition is defined as $\Omega = \bigcup_{\ell=1}^{N} \tau_\ell$ with N the total number of cells. Then the test function space can be defined as

$$\mathcal{V}_h^k = \{v \in L^p(\Omega) : v|_{\tau_\ell} \in \mathbb{Q}_k(\tau_\ell),\ \forall \tau_\ell\}, \tag{4}$$

where $\mathbb{Q}_k(\tau_\ell)$ is the space of tensor product Lagrange polynomials of degree k defined using Gauss points. The discontinuous Galerkin semi-discrete scheme for the Euler equations (1) in each cell τ_ℓ is given by

$$\int_{\tau_\ell} \partial_t \boldsymbol{w}_h v dV - \int_{\tau_\ell} \mathbf{f}(\boldsymbol{w}_h) \cdot \nabla_{\mathbf{x}} v dV + \int_{\partial \tau_\ell} \hat{\mathbf{f}}\left(\boldsymbol{w}_h^-, \boldsymbol{w}_h^+\right) \cdot \vec{\mathbf{n}} v dS = 0, \quad \forall v \in \mathcal{V}_h^k. \tag{5}$$

Since the scheme has to be in conservation form, the boundary terms resulting from the integration by parts need to be computed using a consistent numerical flux $\hat{\mathbf{f}}$, which can be calculated from an exact or approximate solution of a generalized Riemann problem. Additionally the approximated solution $\boldsymbol{w}_h$ is written as a linear combination of functions $\phi_j(x, y)$ from the space $\mathcal{V}_h^k$

$$\boldsymbol{w}_h = \sum_{j=1}^{(k+1)^2} \tilde{\boldsymbol{w}}_j(t) \phi_j(x, y)$$

where $\tilde{\boldsymbol{w}}_j(t)$ are time dependent coefficients. For the full discretization of the problem a time integration strategy has to be selected, thus an explicit strong stability preserving (SSP) Runge-Kutta will be used.

4 Limiting procedures

A limiter procedure is implemented in this paper in order to avoid unphysical oscillations and maintain higher order accuracy in smooth regions. It can be seen as a modification of the slope limiter introduced by Cockburn and Shu [1], which eliminates the oscillations by reducing the order of the polynomial up to a linear function. When P^k polynomial basis functions are used, the linear approximation is calculated just by eliminating the higher order terms of the polynomial. However, for a tensorial product polynomial basis one must follow a different procedure.

The main difference of the limiting procedure proposed in this work is that the average gradients of the states, calculated as

$$\overline{\nabla \boldsymbol{w}_n} = \frac{1}{|\tau_\ell|} \int_{\tau_\ell} \nabla \boldsymbol{w}_n dV$$

are compared component wise with the averaged values of the state variables $\overline{\boldsymbol{w}_n}$ in each element. The modified average gradient $\nabla \boldsymbol{w}_n^{(m)} = \left[\partial_x \boldsymbol{w}_n^{(m)}, \partial_x \boldsymbol{w}_n^{(m)}\right]^T$ is computed as

$$\partial_x \boldsymbol{w}_n^{(m)} = \tilde{m}\left(\overline{\partial_x \boldsymbol{w}_n}, \beta \frac{\Delta_- \overline{\boldsymbol{w}}_n}{\Delta x_n}, \beta \frac{\Delta_+ \overline{\boldsymbol{w}}_n}{\Delta x_n}\right)$$

$$\partial_y \boldsymbol{w}_n^{(m)} = \tilde{m}\left(\overline{\partial_y \boldsymbol{w}_n}, \beta \frac{\Delta_- \overline{\boldsymbol{w}}_n}{\Delta y_n}, \beta \frac{\Delta_+ \overline{\boldsymbol{w}}_n}{\Delta y_n}\right)$$

where $\beta \in [1, 2]$, and

$$\tilde{m}(a_1, ..., a_d) = \begin{cases} a_1, & \text{if } |a_1| \leq Mh^2 \\ minmod(a_1, ..., a_d), & \text{otherwise} \end{cases}$$

is the modified minmod function introduced by Cockburn and Shu [1]. If $\partial_x \boldsymbol{w}_n^{(m)} \neq \overline{\partial_x \boldsymbol{w}_n}$ or $\partial_y \boldsymbol{w}_n^{(m)} \neq \overline{\partial_y \boldsymbol{w}_n}$, then the solution $\boldsymbol{w}_h$ must be reduced to the following linear polynomial

$$\Lambda\Pi_h(\boldsymbol{w}_h)(x, y) = \overline{\boldsymbol{w}_n} + (x - x_n)\partial_x \boldsymbol{w}_n^{(m)} + (y - y_n)\partial_y \boldsymbol{w}_n^{(m)} \tag{6}$$

4.1 Characteristic limiter

The limiter can be applied on characteristic variables which gives more accurate solutions. Compute the right eigenvector matrices $\mathcal{R}_x, \mathcal{R}_y$ and left eigenvector matrices $\mathcal{L}_x, \mathcal{L}_y$ of the corresponding flux Jacobian based on the cell average value $\bar{\boldsymbol{w}}_n$. Define $\boldsymbol{c}_2 = \mathcal{L}_x \overline{\partial_x \boldsymbol{w}_n}$ and $\boldsymbol{c}_3 = \mathcal{L}_y \overline{\partial_y \boldsymbol{w}_n}$. Compute limited quantities by applying the modified minmod function component-wise

$$\tilde{\boldsymbol{c}}_2 = \tilde{m}\left(\boldsymbol{c}_2, \beta \mathcal{L}_x \frac{\Delta_- \overline{\boldsymbol{w}}_n}{\Delta x_n}, \beta \mathcal{L}_x \frac{\Delta_+ \overline{\boldsymbol{w}}_n}{\Delta x_n}\right), \quad \tilde{\boldsymbol{c}}_3 = \tilde{m}\left(\boldsymbol{c}_3, \beta \mathcal{L}_y \frac{\Delta_- \overline{\boldsymbol{w}}_n}{\Delta y_n}, \beta \mathcal{L}_y \frac{\Delta_+ \overline{\boldsymbol{w}}_n}{\Delta y_n}\right)$$

If $\tilde{\boldsymbol{c}}_2 = \boldsymbol{c}_2$ and $\tilde{\boldsymbol{c}}_3 = \boldsymbol{c}_3$ then $\Lambda\Pi_h(\boldsymbol{w}_h) = \boldsymbol{w}_h$ or else the solution is reduced to a linear polynomial as in (6) where $\partial_x \boldsymbol{w}_n^{(m)} = \mathcal{R}_x \tilde{\boldsymbol{c}}_2$ and $\partial_y \boldsymbol{w}_n^{(m)} = \mathcal{R}_y \tilde{\boldsymbol{c}}_3$. Figure 1 shows the solution of a 1-D shock tube problem using limiter on conserved and characteristic variables. We notice that characteristic limiter gives better resolution of discontinuities and also avoids unphysical oscillations.

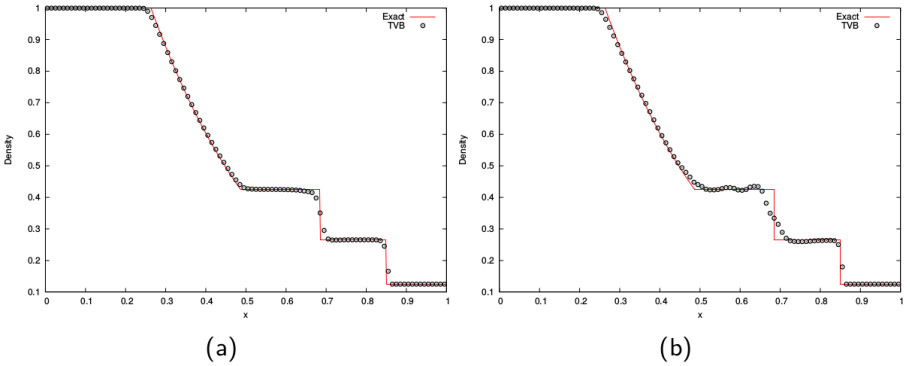

Figure 1: Sod's problem, $k = 1$, 100 cells. (a) Limiting characteristic variables, (b) limiting conserved variables

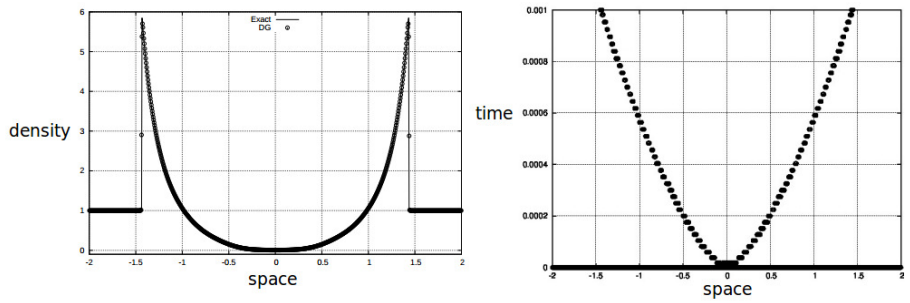

Figure 2: Density of the one-dimensional Sedov blast test problem (up) with shock indicator (down).

4.2 Shock indicator

Krivodonova et al. [2, 3] introduced a way to detect trouble cells where discontinuities may occur. It is known as the KXRCF indicator and is based on the fact that the DG solution shows strong super convergence at the outflow boundary of each element for smooth solutions. To construct such indicator, the cell boundaries are divided into inflow ($\partial\tau_\ell^-$) and outflow ($\partial\tau_\ell^+$) portions. Then, the cell τ_ℓ is believe to contain a discontinuity if

$$\frac{\left|\int_{\partial\tau_\ell^-}\left(w_h^- - w_h^+\right)dS\right|}{h^{\frac{k+1}{2}}\left|\partial\tau_\ell^-\right|\|w_h\|_{\tau_\ell}} > 1,$$

where w_h is a component of the DGM solution $\boldsymbol{w}_h$. Common choices are density, energy and entropy. Some experiments where carried out in one-dimensional problems in order to test the performance of the shock indicator and then verify whether it can be applicable to multi-dimensional problems. Figure 2 shows the case of the Sedov blast wave in one-dimension, and how the shock indicator follows the shock front along the time.

4.3 Positivity preserving limiter

We are interested in physically relevant solution, meaning solution that belongs to the admissible set $\mathcal{U}_{\text{ad}}^{\epsilon}$, where the values of the pressure and density are non negative. Then the numerical solution $\boldsymbol{w}_h(x)$ is to be modified such that $\boldsymbol{w}_h(q) \in \mathcal{U}_{\text{ad}}^{\epsilon}$, $\forall q \in Q$, where Q is a set of quadrature nodes inside the cell and

$$\mathcal{U}_{\text{ad}}^{\epsilon} = \{\boldsymbol{w} \in \mathbb{R}^4 : \rho(\boldsymbol{w}) \geq \epsilon, \quad P(\boldsymbol{w}) \geq \epsilon\}$$

Therefore the positivity preserving limiting procedure by Zhang and Shu [4] is implemented. In order to do so, one has to ensure that the mean value of the density has to be non negative. This is done by setting the CFL condition to a suitable value. Then, $\rho_h \to \hat{\rho}_h$ has to be modified such that $\hat{\rho}_h(q) \geq \epsilon \ \forall q \in Q$, by using the limiter

$$\hat{\rho}_h = \theta_1(\rho_h - \overline{\rho}_n) + \overline{\rho}_n, \quad \theta_1 = \min\left\{\frac{|\overline{\rho}_n - \epsilon|}{|\overline{\rho}_n - \rho_m|}, 1\right\}, \quad \rho_m = \min_{q \in Q} \rho_h(q).$$

which basically shrinks the solution around the mean value, ensuring that every value of the density at the quadrature points is over the $\epsilon-$tolerance. After ensuring the positivity of the density, it is necessary to control the values of the pressure. Denote $\hat{\boldsymbol{w}}_h$, the new state vector such that the density is already positive. If $P(\hat{\boldsymbol{w}}_h(q)) < \epsilon, \forall q \in Q$, a state between $\overline{\boldsymbol{w}}_n$ and $\hat{\boldsymbol{w}}_h(q)$ has to be found such that

$$P((1 - t_q)\overline{\boldsymbol{w}}_n + t_q \hat{\boldsymbol{w}}_h(q)) = \epsilon,$$

where t_q is the unique solution $t_q \in (0, 1)$ of a quadratic equation. Then the modified solution is given by

$$\tilde{\boldsymbol{w}}_h = \theta_2(\hat{\boldsymbol{w}}_h(x) - \overline{\boldsymbol{w}}_n) + \overline{\boldsymbol{w}}_n, \qquad \theta_2 = \min_q t_q.$$

5 Numerical examples

An explicit DG scheme for the Euler system of conservation laws together with the schemes described above was implemented in C++ using the deal.II libraries [5]. It works on a Cartesian grid and uses a third order of accuracy strong stability preserving (SSP) Runge-Kutta scheme.

5.1 Double Mach reflection

This test problem was presented by Woodward and Colella [6] and consists of a Mach 10 planar shock wave in air ($\gamma = 1,4$) which meets a reflecting wall with an angle of 60°. This test case was simulated both without shock indicator (Figure 3) and also with using the KXRCF shock indicator (Figure 4). For this indicator we use the density and the energy as measure variables. In Figure 5 a zoom around the double Mach reflection is shown for three cases (no indicator and using an indicator) together with one of the results from [1]. The shock indicator is able to identify shock regions and apply the limiter only in those regions. The solutions using indicator are of comparable accuracy as in the case of applying slope limiter everywhere, and also compare favorably with the reference solution.

Figure 3: Double Mach reflection test case, polynomial order $k = 2$, $\Delta x = \Delta y = \frac{1}{360}$, without shock indicator.

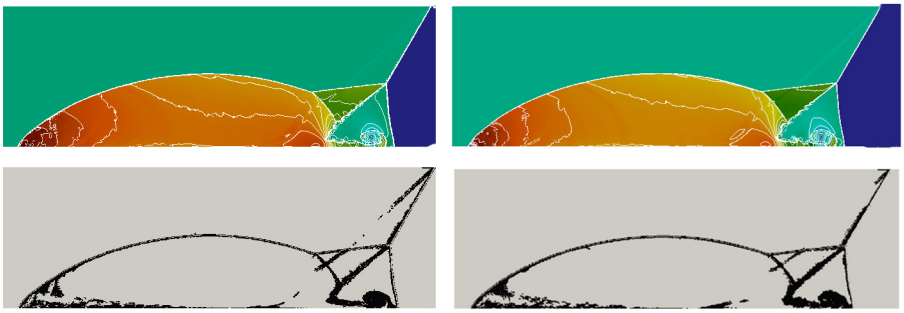

Figure 4: Double Mach reflection test case, polynomial order $k = 2$, $\Delta x = \Delta y = \frac{1}{360}$, with density (left) and energy (right) as shock indicator.

It should be noted that the numerical results presented in this paper have less resolution than the reference case (showed in the lower right corner of figure 5). Nevertheless, the results are comparable.

5.2 Forward facing step

It is a classical test case described in [1]. A right moving Mach 3 fluid enters a wind tunnel, which in turn has a reduction of its height due to a step opposing the direction of the fluid. Figures 6 and 7 show the results after 4 seconds of simulation, without shock indicator, and using density and energy as measure variables for the KXRCF shock indicator respectively. Finally, figure 8 shows a comparison of the level curves from the three cases cited before together with the results shown in [1]. Again we notice that indicator is able to identify shock regions reliably. Moreover it does not identify the slip line which means that limiter is not applied there, leading to good resolution of contact discontinuity.

In this test case, as in the previous one, the numerical results have a lower resolution than the reference solution (showed on the lower right corner of figure 8), however they are competitive results and even present a better behavior at the bottom reflection point of the shock wave.

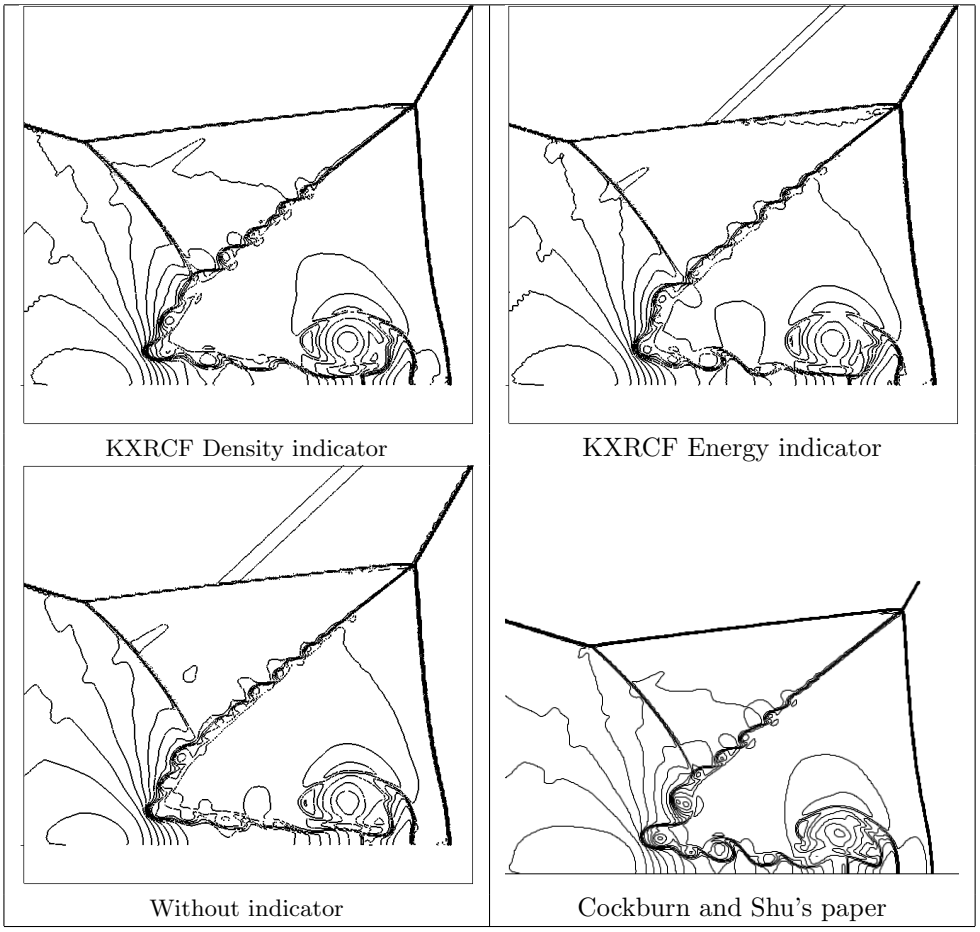

Figure 5: Double Mach reflection zoomed comparison, polynomial order $k = 2$, $\Delta x = \frac{1}{360}$. For the Shu's case the grid size is $\Delta x = \frac{1}{480}$

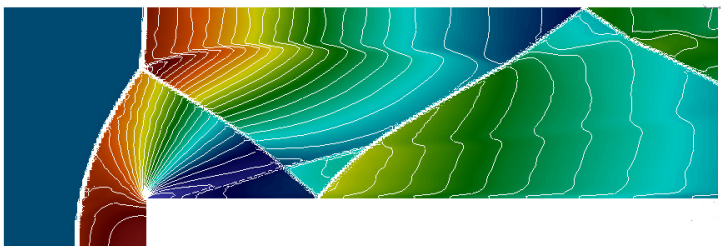

Figure 6: Forward facing step test case, polynomial order $k = 2$, $\Delta x = \Delta y = \frac{1}{100}$, without shock indicator.

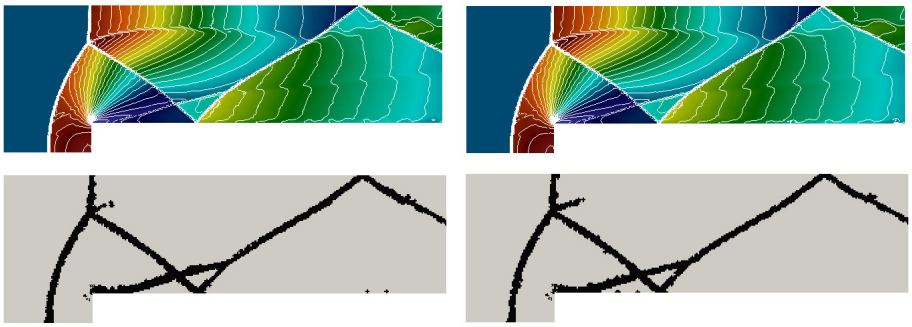

Figure 7: Forward facing step test case, polynomial order $k = 2$, $\Delta x = \Delta y = \frac{1}{100}$, with density (left) and energy (right) as shock indicator.

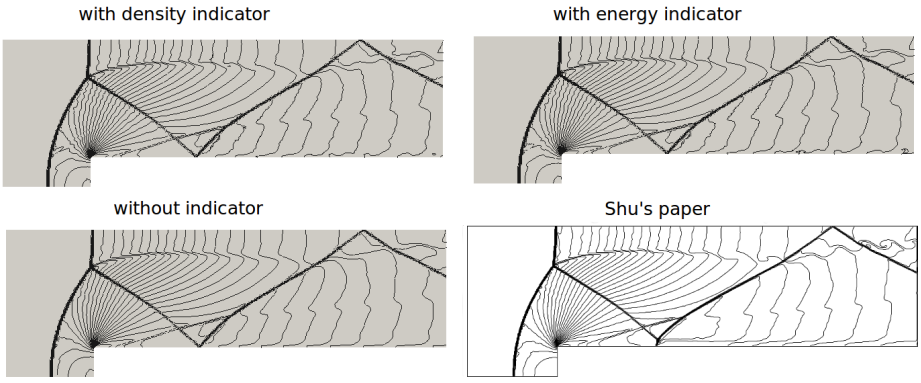

Figure 8: Forward facing step test case comparison, polynomial order $k = 2$, $\Delta x = \frac{1}{100}$. For the result present in Shu's paper the grid size is $\Delta x = \frac{1}{160}$.

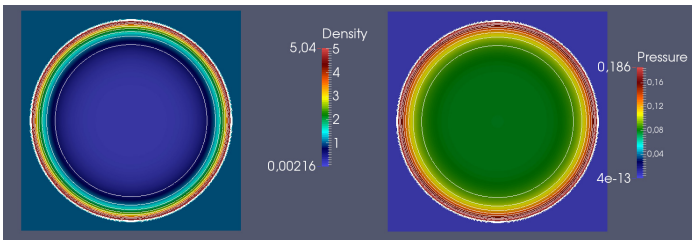

Figure 9: Sedov blast wave 2D test case, polynomial order $k = 2$, $\Delta x = \Delta y = \frac{1}{160}$, without shock indicator.

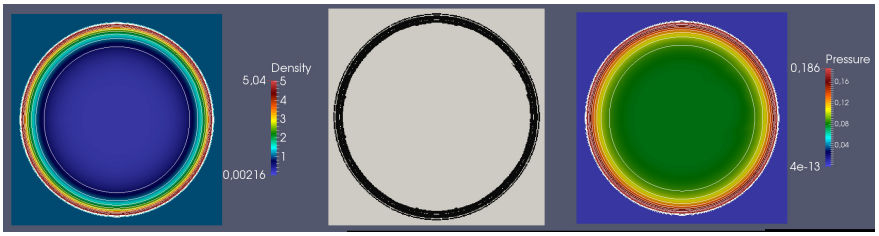

Figure 10: Sedov blast wave 2D test case, polynomial order $k = 2$, $\Delta x = \Delta y = \frac{1}{160}$, with energy as shock indicator.

5.3 Sedov blast wave

This test case is described in [4]. The initial density is $\rho = 1$, velocity is zero and the total energy is equal to 10^{-12} everywhere but in the center of the domain, where it is the constant $\frac{0.979264}{|\tau_\ell|}$. $\gamma = 1.4$. The energy concentrated generates a shock wave that propagates radially with time. Because of its nearly-vacuum conditions, it is used to test whether the positivity of variables is preserved with the scheme. Figures 9 and 10 show the profiles of the density and the energy after 1 second of simulation, without shock indicator and using energy as measure variable for the KXRCF shock indicator respectively. When the density is used as measured variable in the shock indicator, due to its constant initial value, the code crashes after one time step failing to detect the shock. The energy which involves all variables is a better choice in this case.

6 Conclusions

We have built an algorithm and a C++ implementation to solve numerically the compressible Euler equations, using a discontinuous Galerkin method. An adaptation of the slope limiter was proposed for tensorial product polynomial basis in order to control oscillations for discontinuous solutions, and in order to preserve positivity of the variables (density and pressure) a bound preserving limiter was implemented. The KXRCF shock indicator seems to detect well the locations of the shocks in the 2D examples, however special care has to be taken in the selection of the measured variable as it was shown in the Sedov blast wave test case. The implementation of the shock indicator can be justified as it

avoids the usage of limiters all over the domain, which in turn may lead to an improvement in the performance of the algorithm. These numerical algorithms are useful for astrophysical applications where high accuracy is required in problems where density or pressure may become very low in some regions which is part of our future work.

Acknowledgments

PC thanks the Airbus Foundation Chair at TIFR-CAM, Bangalore, for support in carrying out this work. JP G-V thanks the GRK 1147 for its support. CK thanks the SPPEXA priority program of the German Science Foundation (DFG).

References

[1] B. Cockburn and C. W. Shu, J. Comput. Phys. **141**, 199 - 224 (1998).

[2] J. E. Flaherty, L. Krivodonova, J.-F. Remacle and M. S. Shephard, Finite Element Anal. Design **38**, 889 – 908 (2002).

[3] L. Krivodonova, J. Xin, J.-F. Remacle, N. Chevaugeon and J. E. Flaherty, Apl. Num. Math. **48**, 323 – 338 (2004).

[4] X. Zhang, and C. W. Shu, J. Comput. Phys. **229**, 8918 – 8934 (2010),

[5] W. Bangerth and R. Hartmann and G. Kanschat ACM Trans. Math. Softw. **33** No. 4, 24/1 – 24/27 (2007),

[6] P.R. Woodward and P. Colella, J. Comput. Phys. **54**, 115 – 173 (1984).

[7] J. P. Gallego-Valencia, J. Löbbert, S. Müthing, P. Bastian, C. Klingenberg, and Y. Xia, Proc. in App. Math. and Mech. **14**, 953 – 954 (2014).